APL Materials

a-axis $YBa_2Cu_3O_{7-x}$/$PrBa_2Cu_3O_{7-x}$/$YBa_2Cu_3O_{7-x}$ trilayers with subnanometer rms roughness

Cite as: APL Mater. **9**, 021117 (2021); https://doi.org/10.1063/5.0034648
Submitted: 22 October 2020 . Accepted: 06 January 2021 . Published Online: 17 February 2021

Y. Eren Suyolcu, Jiaxin Sun, Berit H. Goodge, Jisung Park, Jürgen Schubert, Lena F. Kourkoutis, and Darrell G. Schlom

a-axis $YBa_2Cu_3O_{7-x}/PrBa_2Cu_3O_{7-x}/YBa_2Cu_3O_{7-x}$ trilayers with subnanometer rms roughness

Cite as: APL Mater. 9, 021117 (2021); doi: 10.1063/5.0034648
Submitted: 22 October 2020 • Accepted: 6 January 2021 •
Published Online: 17 February 2021

Y. Eren Suyolcu,[1,a] Jiaxin Sun,[1] Berit H. Goodge,[2] Jisung Park,[1] Jürgen Schubert,[3] Lena F. Kourkoutis,[2,4] and Darrell G. Schlom[1,4,5,a]

AFFILIATIONS

[1] Department of Materials Sciences and Engineering, Cornell University, Ithaca, New York 14853, USA
[2] School of Applied and Engineering Physics, Cornell University, Ithaca, New York 14853, USA
[3] Peter Grünberg Institute (PGI-9) and JARA-Fundamentals of Future Information Technology, Forschungszentrum Jülich GmbH, 52425 Jülich, Germany
[4] Kavli Institute at Cornell for Nanoscale Science, Ithaca, New York 14853, USA
[5] Leibniz-Institut für Kristallzüchtung, Max-Born-Str. 2, 12489 Berlin, Germany

[a] **Authors to whom correspondence should be addressed:** eren.suyolcu@cornell.edu and schlom@cornell.edu

ABSTRACT

We demonstrate *a*-axis $YBa_2Cu_3O_{7-x}/PrBa_2Cu_3O_{7-x}/YBa_2Cu_3O_{7-x}$ trilayers grown on (100) $LaAlO_3$ substrates with improved interface smoothness. The trilayers are synthesized by ozone-assisted molecular-beam epitaxy. The thickness of the $PrBa_2Cu_3O_{7-x}$ layer is held constant at 8 nm, and the thickness of the $YBa_2Cu_3O_{7-x}$ layers is varied from 24 nm to 100 nm. X-ray diffraction measurements show all trilayers to have >97% *a*-axis content. The rms roughness of the thinnest trilayer is <0.7 nm, and this roughness increases with the thickness of the $YBa_2Cu_3O_{7-x}$ layers. The thickness of the $YBa_2Cu_3O_{7-x}$ layers also affects the transport properties: while all samples exhibit an onset of the superconducting transition at and above 85 K, the thinner samples show wider transition widths, ΔT_c. High-resolution scanning transmission electron microscopy reveals coherent and chemically sharp interfaces and that growth begins with a cubic $(Y,Ba)CuO_{3-x}$ perovskite phase that transforms into *a*-axis oriented $YBa_2Cu_3O_{7-x}$ as the substrate temperature is ramped up.

Shortly after the discovery of high-temperature superconductivity in $YBa_2Cu_3O_7$,[1,2] measurements showed that the superconducting proximity length along the *a*-axis ($\xi_a \approx 1.1$ nm)[3,4] of $YBa_2Cu_3O_{7-x}$ is nearly an order of magnitude longer than along the *c*-axis ($\xi_c \approx 0.1$ nm).[4,5] Note that ξ_c is shorter than the distance between the CuO_2 planes. This difference makes the *a*-axis direction relevant to forming controlled and reproducible $YBa_2Cu_3O_{7-x}$ based Josephson junctions (JJs) for superconducting electronics.[6] Most JJs in $YBa_2Cu_3O_{7-x}$ have been made using epitaxial $YBa_2Cu_3O_{7-x}$ films oriented with the *c*-axis perpendicular to the film surface.[7] This is because such films, referred to as *c*-axis oriented films, exhibit the highest superconducting transition temperature (T_c), highest critical current density (J_c), and smoothest surface. JJs in such films are made in the (001) plane to exploit the longer in-plane coherence length, ξ_a. They occur at weak links present at grain boundaries[8–12] or formed by helium ion bombardment.[13] They are also made by introducing tunnel barriers by a ramp-junction process that involves patterning the *c*-axis $YBa_2Cu_3O_{7-x}$ film followed by epitaxial regrowth.[11,14,15]

A more direct approach to fabricate high quality JJs—one that involves pristine interfaces formed without breaking vacuum—is through the growth of $YBa_2Cu_3O_{7-x}$ films oriented with the *a*-axis perpendicular to the film surface (i.e., *a*-axis oriented films). This was recognized early on and numerous groups developed methods to grow *a*-axis oriented films[16,17] as well as JJs based upon them, e.g., *a*-axis oriented $YBa_2Cu_3O_{7-x}/PrBa_2Cu_3O_{7-x}/YBa_2Cu_3O_{7-x}$ trilayers.[6,18] Although JJs were successfully fabricated, the resulting junctions were neither controlled nor reproducible due to the significant roughness of the *a*-axis oriented $YBa_2Cu_3O_{7-x}$ films.[18] Note that the low-energy surface of $YBa_2Cu_3O_{7-x}$ is the (001) plane,[19]

explaining the far smoother morphology of *c*-axis $YBa_2Cu_3O_{7-x}$ films compared to *a*-axis $YBa_2Cu_3O_{7-x}$ films.

To improve the quality of *a*-axis $YBa_2Cu_3O_{7-x}$ films and heterostructures, several techniques have been employed when using $PrBa_2Cu_3O_{7-x}$ as either a buffer layer or a barrier layer.[20] These include increasing the substrate temperature, either gradually[21] or with a step-like ramp after the *a*-axis buffer layer has nucleated,[6,20,22,23] and even performing this in tandem with ramping down the background oxidant gas pressure.[21,24,25] Nonetheless, the interface roughness has remained a major challenge for samples showing good superconducting transitions [e.g., an rms of ~10 nm for *a*-axis $YBa_2Cu_3O_{7-x}$ grown on (100) $LaAlO_3$][21] as has avoiding the unwanted nucleation of *c*-axis $YBa_2Cu_3O_{7-x}$ or $PrBa_2Cu_3O_{7-x}$ when the temperature is ramped.[22,23] The smoothest *a*-axis $YBa_2Cu_3O_{7-x}$ (or $DyBa_2Cu_3O_{7-x}$) films reported were grown utilizing ozone-assisted molecular-beam epitaxy (MBE), and rms surface roughnesses as low as 0.4 nm were achieved.[25–27] This promising smoothness motivated the current work to utilize MBE to make *a*-axis $YBa_2Cu_3O_{7-x}/PrBa_2Cu_3O_{7-x}/YBa_2Cu_3O_{7-x}$ trilayers.

Following the initial pioneering studies on *a*-axis $YBa_2Cu_3O_{7-x}/PrBa_2Cu_3O_{7-x}/YBa_2Cu_3O_{7-x}$ trilayers and a recognition of the challenges involved in making a viable JJ technology by this approach, work on this system has all but ceased. Now decades later, we revisit this challenge harnessing the improvements that have been made in the intervening years in thin film growth methods. Using MBE, we grow *a*-axis $YBa_2Cu_3O_{7-x}/PrBa_2Cu_3O_{7-x}/YBa_2Cu_3O_{7-x}$ trilayers paying particular attention to growth conditions that yield smooth surfaces. We study the thickness dependence of the surface roughness as well as the superconducting transition width. Our results, including cross-sectional scanning transmission electron microscopy with electron energy loss spectroscopy (STEM-EELS) to characterize the interfaces with chemical specificity, demonstrate that the interface roughness can be decreased significantly to a level comparable to the thickness of relevant tunneling barrier layers. The substantial improvement in interface smoothness that we observe in *a*-axis $YBa_2Cu_3O_{7-x}/PrBa_2Cu_3O_{7-x}/YBa_2Cu_3O_{7-x}$ trilayers suggests that *a*-axis $YBa_2Cu_3O_{7-x}$-based JJs with requisite smoothness to provide the precise thickness control of the tunnel barrier needed for a JJ technology are achievable.

$YBa_2Cu_3O_{7-x}/PrBa_2Cu_3O_{7-x}/YBa_2Cu_3O_{7-x}$ trilayers with 24 nm, 32 nm, 64 nm, and 100 nm thick $YBa_2Cu_3O_{7-x}$ layers, in which the $PrBa_2Cu_3O_{7-x}$ layer thickness is kept constant at 8 nm, were grown on 10 × 10 mm^2 (100)-oriented $LaAlO_3$ substrates by ozone-assisted MBE [Fig. 1(a)]. Although high quality *a*-axis $YBa_2Cu_3O_{7-x}$

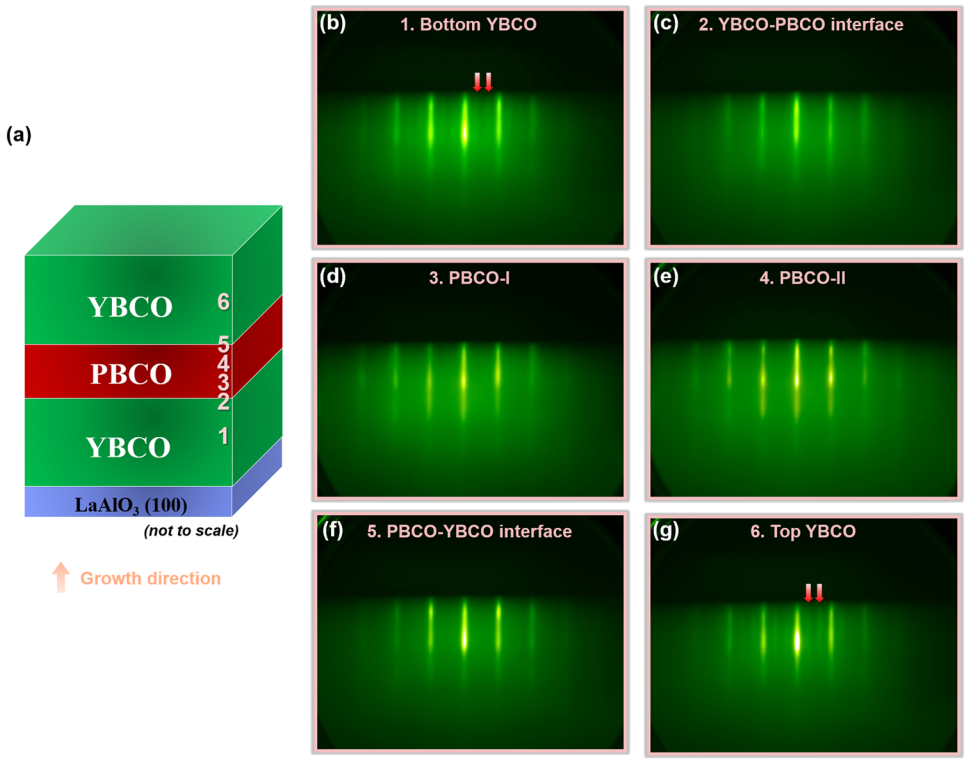

FIG. 1. (a) Schematic of the $YBa_2Cu_3O_{7-x}/PrBa_2Cu_3O_{7-x}/YBa_2Cu_3O_{7-x}$ trilayers grown on (100) $LaAlO_3$ substrates. [(b)–(g)] Real-time RHEED images acquired along the [010] azimuth of the (100) $LaAlO_3$ substrate during the growth of the 24 nm $YBa_2Cu_3O_{7-x}$/8 nm $PrBa_2Cu_3O_{7-x}$/24 nm $YBa_2Cu_3O_{7-x}$ trilayer at six different times schematically illustrated in (a). The RHEED patterns are from the bottom $YBa_2Cu_3O_{7-x}$ layer (b), $YBa_2Cu_3O_{7-x}/PrBa_2Cu_3O_{7-x}$ interface (c), $PrBa_2Cu_3O_{7-x}$ layer (d) and (e), $PrBa_2Cu_3O_{7-x}/YBa_2Cu_3O_{7-x}$ interface, and (f) top $YBa_2Cu_3O_{7-x}$ layer. The red arrows added to (b) and (g) point to the diffraction streaks associated with the *c*-axis of the $YBa_2Cu_3O_{7-x}$ lying in-plane.

films have been grown on (100) $LaSrGaO_4$ substrates,[28] we used (100) $LaAlO_3$ substrates in this work because our goal is to identify a path that can be scaled to large diameters to enable its translation to a viable technology. 3-in. diameter $LaAlO_3$ substrates are currently available; in the past, even 4-in. diameter $LaAlO_3$ substrates were commercially produced.[29]

The $YBa_2Cu_3O_{7-x}$/$PrBa_2Cu_3O_{7-x}$/$YBa_2Cu_3O_{7-x}$ trilayers were synthesized in a Veeco GEN10 MBE. Yttrium (99.6%), barium (99.99%), praseodymium (99.1%), and copper (99.99%) were evaporated from thermal effusion cells with fluxes of 1.1×10^{13} cm^{-2} s^{-1}, 2.2×10^{13} cm^{-2} s^{-1}, and 3.3×10^{13} cm^{-2} s^{-1}, respectively. Prior to growth, the (100) $LaAlO_3$ substrates (CrysTec GmbH) were etched in boiling water, annealed at 1300 °C in air for 10 h, and then etched again in boiling water to obtain an AlO_2-terminated surface with a step-and-terrace morphology.[30] Following this surface treatment, the backside of the (100) $LaAlO_3$ substrates were coated with a 10 nm thick titanium adhesion layer followed by 200 nm of platinum, enabling the otherwise transparent substrates to be radiatively heated during MBE growth. The $YBa_2Cu_3O_{7-x}$ (or $PrBa_2Cu_3O_{7-x}$) layers were grown by simultaneously depositing yttrium (or praseodymium), barium, and copper onto the heated substrate under a continuous flux of distilled ozone (~80% O_3 + 20% O_2) yielding a background pressure of 1×10^{-6} Torr. After growth, the samples were cooled to under 100 °C in the same pressure of distilled ozone in which they were grown before turning off the ozone molecular beam and removing the samples from vacuum.

Because $YBa_2Cu_3O_{7-x}$ is a point compound that is unable to accommodate appreciable off-stoichiometry,[31] flux calibration presents a significant challenge where secondary impurity phases nucleate easily and significantly degrade film quality.[32] We tackle this challenge by separately calibrating the flux of each element by growing binary oxides of the constituents, namely, Y_2O_3, PrO_2, BaO, and CuO. From these separate binary flux calibrations, the temperatures of the effusion cells containing yttrium, barium, praseodymium, and copper are adjusted to match the desired 1:2:3 flux ratio among Y(Pr):Ba:Cu. The temperature of the substrate is measured during growth by using a thermocouple (T_{Tc}) that is positioned close to but not in direct contact with the substrate and an optical pyrometer (T_{Pyr}) operating at a wavelength of 1550 nm. The growth of the trilayers starts at low-temperature, $T_{Tc} \approx 420$ °C ($T_{Pyr} \approx 530$ °C), resulting in a cubic perovskite (Y,Ba)CuO_{3-x} phase[33] for the first few layers and ends at $T_{Tc} \approx 570$ °C ($T_{Pyr} \approx 620$ °C) following a temperature-ramping procedure. The details of the flux calibration method (including the characterization of individual binary oxides) are presented in Figs. S1–S5 of the supplementary material. Also shown are the temperature-ramping details and the *in situ* reflection high-energy electron diffraction (RHEED) characterization of a reference *a*-axis $YBa_2Cu_3O_{7-x}$ single-phase film grown as part of the optimization of the growth procedure (Fig. S6).

During growth, the films were monitored by *in situ* RHEED with KSA-400 software and a Staib electron gun operating at 13 kV and 1.45 A. RHEED images taken during the growth of the 24 nm $YBa_2Cu_3O_{7-x}$/8 nm $PrBa_2Cu_3O_{7-x}$/24 nm $YBa_2Cu_3O_{7-x}$ trilayer are shown in Figs. 1(b)–1(g). The structural quality and the *a*-axis/*c*-axis ratio of the samples was explored using a PANalytical Empyrean x-ray diffractometer (XRD) at 45 kV and 40 mA with Cu $K\alpha_1$ radiation (1.54057 Å). For surface morphological characterization of the films, *ex situ* atomic force microscopy (AFM) measurements were conducted using an Asylum Cypher ES Environmental AFM system. Resistance as a function of temperature measurements were carried out using a homemade four-point van der Pauw geometry system that slowly dips the samples into a Dewar of liquid helium.

Detailed investigations of the films were conducted using atomic-resolution scanning transmission electron microscopy (STEM). Cross-sectional TEM specimens were prepared by focused ion beam (FIB) lift-out with a Thermo Fisher Helios G4 UX Dual Beam system. The samples were imaged on an aberration-corrected FEI Titan Themis at 300 kV. STEM high-angle annular dark-field (HAADF) imaging was performed with a probe convergence semi-angle of 21.4 mrad and inner and outer collection angles from 68 mrad to 340 mrad. STEM electron energy loss spectroscopy (EELS) measurements were performed on the same Titan system equipped with a 965 GIF Quantum ER and Gatan K2 Summit direct detector operated in the electron counting mode, with a beam current of ~50 pA and scan times of 2.5 ms or 5 ms per 0.4 Å pixel. A multivariate weighted principal component analysis routine (MSA Plugin in Digital Micrograph) is used to decrease the noise level in STEM data.[34]

The structural quality of the samples is assessed by XRD measurements. In the coupled θ–2θ XRD scans in Fig. 2(a), only $h00$, $0k0$, and 00ℓ reflections of the $YBa_2Cu_3O_{7-x}$ and $PrBa_2Cu_3O_{7-x}$ phases are indexed, indicating that the film only contains phases with the desired stoichiometry; they are free of impurity phases associated with off-stoichiometry. With increasing $YBa_2Cu_3O_{7-x}$ layer thicknesses, 00ℓ reflections emerge showing the nucleation and propagation of *c*-axis grains in the films. Off-axis ϕ scans of the 102 family of reflections of the orthorhombic $YBa_2Cu_3O_{7-x}$/$PrBa_2Cu_3O_{7-x}$ at $\chi \approx 56.8°$ and $\chi \approx 33.2°$ are used to measure the *a*-axis and *c*-axis content of the orthorhombic grains, respectively. Note that $\chi = 90°$ aligns the diffraction vector to be perpendicular to the plane of the substrate.[35] In the 102 ϕ scan of the trilayer sample shown in Fig. 2(b), four peaks associated with the *a*-axis grains are observed corresponding to 90° in-plane rotational twinning: the *c*-axis of the $YBa_2Cu_3O_{7-x}$ and $PrBa_2Cu_3O_{7-x}$ is aligned parallel to the [010] direction of the (100) $LaAlO_3$ substrate in one set of twin domains and parallel to the [001] direction of the (100) $LaAlO_3$ substrate in the other set of twin domains.[17,20,36,37] No intensity associated with *c*-axis grains is observed, indicating that the film contains no *c*-axis grains within the resolution of our XRD scan. The off-axis ϕ scans of all trilayer samples shown in Fig. S5 indicate that all four trilayers have more than 97% *a*-axis content in the Y(Pr)$Ba_2Cu_3O_{7-x}$ orthorhombic phase. In addition to the orthorhombic phases, we also observe a cubic perovskite phase. This phase has been previously reported in the literature as a low-temperature, kinetically stabilized *I*-centered cubic phase[38] or primitive simple-cubic phase.[39] The formation of this phase and its role in stabilizing the *a*-axis $YBa_2Cu_3O_{7-x}$/$PrBa_2Cu_3O_{7-x}$/$YBa_2Cu_3O_{7-x}$ trilayers are discussed below in tandem with its observation by HAADF-STEM. In the reciprocal space map (RSM) around the $LaAlO_3$ $\bar{1}03$ reflection (pseudocubic) in Fig. 2(c), we also observe a perovskite-like $\bar{1}03$ reflection [denoted *p*-(Y,Ba)CuO_{3-x}] and the orthorhombic phase $30\bar{3}/3\bar{1}0$ and $033/\bar{1}30$ reflections

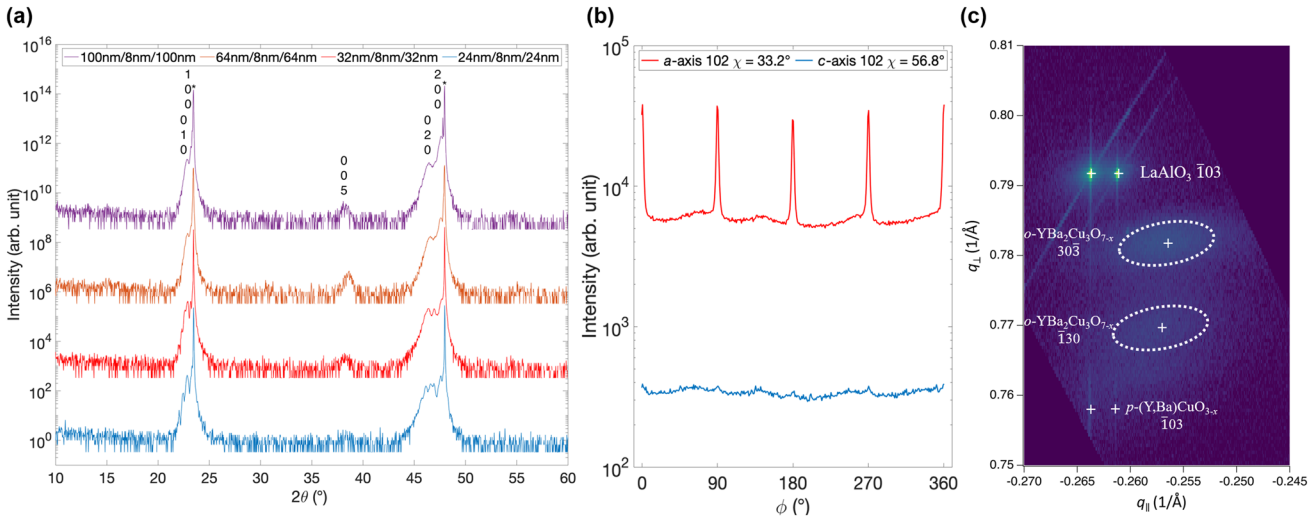

FIG. 2. X-ray diffraction. (a) θ–2θ scans of trilayers with different $YBa_2Cu_3O_{7-x}$ layer thicknesses showing only $h00$, $0k0$, and 00ℓ reflections. Symbol * denotes substrate reflections. To offset the scans for clarity, the 32 nm/8 nm/32 nm, 64 nm/8 nm/64 nm, and 100 nm/8 nm/100 nm scan intensities were multiplied by factors of 10^3, 10^6, and 10^9, respectively. (b) Off-axis ϕ scans of the 102 family of peaks at $\chi \approx 56.8°$ (red) and $\chi \approx 33.2°$ (blue) of the thin trilayer (24 nm/8 nm/24 nm) showing the absence of *c*-axis grains. To offset the scan for clarity, the *a*-axis scan intensity was multiplied by 10. (c) RSM around the $LaAlO_3$ $\bar{1}03$ peak of the thin sample showing the *a*-axis and *b*-axis orthorhombic peaks $30\bar{3}$ and $\bar{1}30$, as well as the perovskite $(Y,Ba)CuO_{3-x}\bar{1}03$ peak. The "+" symbol and dashed ellipsoids are used to highlight the reflections.

associated with the *a*-axis and *b*-axis $YBa_2Cu_3O_{7-x}$ grains, respectively.

The surface morphologies of the same as-grown $YBa_2Cu_3O_{7-x}/PrBa_2Cu_3O_{7-x}/YBa_2Cu_3O_{7-x}$ trilayers were established by *ex situ* AFM using tapping mode. With increasing $YBa_2Cu_3O_{7-x}$ layer thickness, the elongated $YBa_2Cu_3O_{7-x}$ grains as well as the in-plane 90° rotational twinning of these rectangular-shaped features become visible in the $2 \times 2\ \mu m^2$ topography scans presented in Figs. 3(a)–3(d). This morphology arises from the much slower growth rate of $YBa_2Cu_3O_{7-x}$ grains along [001] than in the (001) plane.[40] The root-mean-square (rms) roughness also increases with increasing $YBa_2Cu_3O_{7-x}$ layer thickness from 0.62 nm in the thinnest 24 nm/8 nm/24 nm trilayer to 2.3 nm in the thickest 100 nm/8 nm/100 nm trilayer. Surface roughness is an important metric affecting the yield and electrical performance of $YBa_2Cu_3O_{7-x}$-based JJs involving extrinsic interfaces, i.e., tunnel barriers. The 0.62 nm rms roughness we observe is the smoothest reported in the literature and a significant reduction from the 11.3 nm measured previously on *a*-axis $YBa_2Cu_3O_{7-x}/PrBa_2Cu_3O_{7-x}$ bilayers with 270 nm thick $YBa_2Cu_3O_{7-x}$ layers grown on (100) $LaAlO_3$ substrates.[21]

The resistance as a function of temperature (R–T) was measured on the same $YBa_2Cu_3O_{7-x}/PrBa_2Cu_3O_{7-x}/YBa_2Cu_3O_{7-x}$ trilayers; the results are presented in Fig. 4. As is evident from the R–T plots in Fig. 4(a), all trilayers superconduct. The normal state resistance decreases and the onset temperature of the superconducting transition (T_{onset}) increases with increasing $YBa_2Cu_3O_{7-x}$ layer thickness—from 85 K for the 24 nm/8 nm/24 nm trilayer to 90 K for the 100 nm/8 nm/100 nm trilayer, as shown in Fig. 4(b). We define T_{onset} as the temperature at which the resistance falls below a linear extrapolation of the R vs T behavior from its slope in the 200 K–300 K regime. The superconducting transition width (ΔT_c), here defined as the temperature difference between T_{onset} and the temperature at which the resistance is zero (within the noise of our measurement), ΔT_c, decreases with increasing $YBa_2Cu_3O_{7-x}$ layer thickness from 29 K for the 24 nm/8 nm/24 nm trilayer to 10 K for the 100 nm/8 nm/100 nm trilayer, as seen in Fig. 4(c). Compared to *c*-axis $YBa_2Cu_3O_{7-x}$ films, however, these transition widths are still relatively broad.[41] Such behavior is ubiquitous in twinned *a*-axis $YBa_2Cu_3O_{7-x}$ films,[17,20,21,24] especially when the thickness of the *a*-axis $YBa_2Cu_3O_{7-x}$ is under 100 nm.[18,42] A portion of the broad transitions observed might be intrinsic, as is the case for interface superconductivity at $La_{2-x}Sr_xCuO_4$—La_2CuO_4 interfaces.[43] In the present case, an intrinsic contributor could be the generation and flow of Josephson vortices in the vicinity of T_c.[44,45] Extrinsic contributions to the broadening likely arise from local disorder and inhomogeneities in the samples, insufficient oxidation, and the degradation of the samples over time.[46]

To reveal the microstructure and interface abruptness of the samples, we studied two trilayer samples with cross-sectional high-resolution STEM. A low-magnification HAADF-STEM image of the 24 nm/8 nm/24 nm $YBa_2Cu_3O_{7-x}/PrBa_2Cu_3O_{7-x}/YBa_2Cu_3O_{7-x}$ trilayer shown in Fig. 5(a) is representative of the complete sample. Individual layers are distinguished as darker and brighter regions due to the atomic number (Z) contrast[47] of HAADF imaging. The $PrBa_2Cu_3O_{7-x}$ layer gives brighter contrast compared to the $YBa_2Cu_3O_{7-x}$ layer because praseodymium ($Z_{Pr} = 59$) is heavier than yttrium ($Z_Y = 39$). The $LaAlO_3$ substrate also shows relatively bright contrast for the same reason ($Z_{La} = 57$). A higher magnification image [Fig. 5(b)] focusing on a representative interface region reveals that the interfaces in the $YBa_2Cu_3O_{7-x}/PrBa_2Cu_3O_{7-x}/YBa_2Cu_3O_{7-x}$ trilayer are

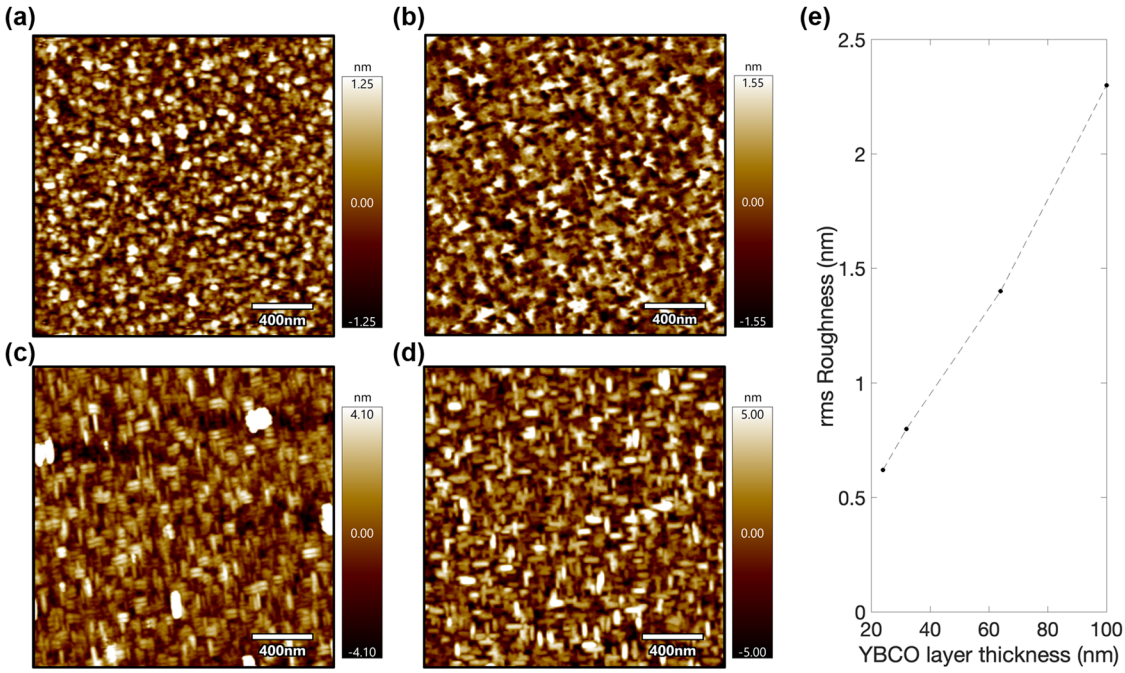

FIG. 3. Surface morphology of the $YBa_2Cu_3O_{7-x}/PrBa_2Cu_3O_{7-x}/YBa_2Cu_3O_{7-x}$ trilayers revealed by AFM. [(a)–(d)] 2 × 2 μm^2 topography scans of the 24 nm/8 nm/24 nm, 32 nm/8 nm/32 nm, 64 nm/8 nm/64 nm, and 100 nm/8 nm/100 nm trilayers measured utilizing tapping mode, respectively. (e) rms roughness calculated from (a)–(d) as a function of the $YBa_2Cu_3O_{7-x}$ layer thickness. The dotted line is a guide to the eye.

coherent. Neither in low-magnification nor in high-magnification scans were *c*-axis grains observed in our STEM images, consistent with the high volume fraction of *a*-axis growth measured by XRD. Nevertheless, structural coherence does not prove chemical abruptness at interfaces involving cuprate high-temperature superconductors.[48,49]

The chemical abruptness of the $YBa_2Cu_3O_{7-x}/PrBa_2Cu_3O_{7-x}/YBa_2Cu_3O_{7-x}$ interfaces was assessed by atomic-resolution elemental mapping via STEM-EELS. Figures 5(c)–5(e) show the elemental maps obtained using Pr–$M_{5,4}$ (red), Y–$L_{3,2}$ (green), and Ba–$M_{5,4}$ (blue) edges in the region outlined by the tan rectangle in Fig. 5(a). A red, green, blue (RGB) overlay of the elemental maps from this region is shown in Fig. 5(f), while Fig. 5(g) shows the simultaneously acquired ADF-STEM image of the same region. Atomic-resolution EELS maps reveal abrupt interface profiles, corroborating the STEM-HAADF images. Both interfaces show minimal Y–Pr intermixing, although some asymmetry of the interface profiles is seen. The lower $YBa_2Cu_3O_{7-x}/PrBa_2Cu_3O_{7-x}$ interface shows a nearly perfect interface profile free of Y–Pr intermixing; the upper interface ($PrBa_2Cu_3O_{7-x}/YBa_2Cu_3O_{7-x}$) presents a slightly rougher local profile with a roughness limited to 1–2 monolayers.

The roughness of the interfaces revealed by HAADF-STEM and STEM-EELS in Fig. 5 is consistent with the qualitative observations made during growth by *in situ* RHEED [Figs. 1(b)–1(g)] of this same $YBa_2Cu_3O_{7-x}/PrBa_2Cu_3O_{7-x}/YBa_2Cu_3O_{7-x}$ trilayer. The arrowed streaks of *a*-axis oriented $YBa_2Cu_3O_{7-x}$ in Fig. 1(b) promptly disappear in transitioning from the lower $YBa_2Cu_3O_{7-x}$ layer to the $PrBa_2Cu_3O_{7-x}$ barrier layer in Fig. 1(c), indicating that the $PrBa_2Cu_3O_{7-x}$ barrier layer uniformly covers the lower $YBa_2Cu_3O_{7-x}$ layer. At the upper interface, however, it takes noticeably longer for the arrowed streaks of the upper $YBa_2Cu_3O_{7-x}$ layer to reappear [Figs. 1(f) and 1(g)]. Furthermore, the time that it takes for the arrowed streaks of *a*-axis oriented $YBa_2Cu_3O_{7-x}$ to reappear in going from the $PrBa_2Cu_3O_{7-x}$ barrier to the $YBa_2Cu_3O_{7-x}$ upper layer takes progressively longer for the thicker trilayers. This is consistent with the increased surface roughness seen by AFM in Fig. 3 as the thickness of the $YBa_2Cu_3O_{7-x}$ layers increases.

In addition to the coherent and chemically sharp interfaces, some defects were observed by STEM. For example, intergrowths of an extra Cu–O layer intercalated into the $YBa_2Cu_3O_{7-x}$ structure to locally form $YBa_2Cu_4O_{8-x}$ (Fig. S7) are seen. Such intergrown layers are well-known and common in $YBa_2Cu_3O_{7-x}$—in bulk, thin-films, and heterostructures.[50–52]

The cross-sectional HAADF-STEM imaging also unveils the location of the cubic perovskite $(Y,Ba)CuO_{3-x}$ phase detected in the XRD measurements. The thickness of the cubic $(Y,Ba)CuO_{3-x}$ layer is found to be ~10 nm, and it is located under the bottom $YBa_2Cu_3O_{7-x}$ layer [Fig. S7(a)]. This cubic $(Y,Ba)CuO_{3-x}$ layer forms at the start of growth when the substrate is coldest and surface diffusion is most constrained. Yttrium and barium are unable to diffuse sufficiently far to establish the Y–Ba–Ba–. . . ordered arrangement found in the unit cell of $YBa_2Cu_3O_{7-x}$; instead, yttrium and

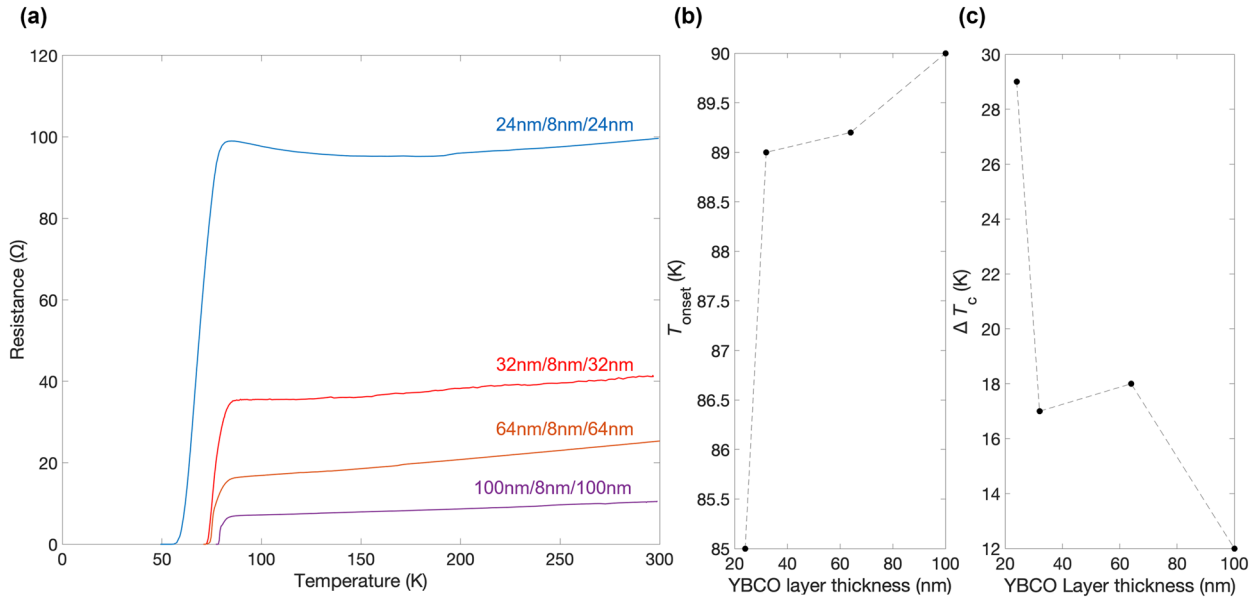

FIG. 4. Transport properties of the same $YBa_2Cu_3O_{7-x}/PrBa_2Cu_3O_{7-x}/YBa_2Cu_3O_{7-x}$ trilayers. (a) Resistance as a function of temperature, (b) onset of the superconducting transition (T_{onset}) as a function of $YBa_2Cu_3O_{7-x}$ layer thickness, and (c) superconducting transition width (ΔT_c) as a function of $YBa_2Cu_3O_{7-x}$ layer thickness. The dotted lines are guides to the eye.

barium share the *A*-site of the resulting perovskite structure, with copper on the *B*-site.[53]

As the temperature of the substrate is ramped, the diffusion lengths increase, and in-plane structural order emerges. The resulting *a*-axis $YBa_2Cu_3O_{7-x}$ grains grow epitaxially in one of two symmetry equivalent orientations: with the *c*-axis parallel to either [010] or [001] of the cubic $(Y,Ba)CuO_{3-x}$ layer on which they nucleate on the (100) $LaAlO_3$ substrate. One set of such domains is clearly seen in Fig. S7: the set with the *c*-axis along the horizontal direction of the image. The other set, with the *c*-axis oriented into the plane of the image, is more difficult to establish because the spacing of these domains along the horizontal direction is the same perovskite spacing as the cubic $(Y,Ba)CuO_{3-x}$ layer on which these domains nucleated.

Our hypothesis is that the ~10 nm thick cubic $(Y,Ba)CuO_{3-x}$ layer only lies under the *a*-axis oriented $YBa_2Cu_3O_{7-x}$ layer and that the regions in which this perovskite structure appears to extend further, i.e., through and all the way to the surface of the trilayer, are actually the set of *a*-axis domains oriented with the *c*-axis running into the plane of the image. This hypothesis is consistent with the grain size of the *a*-domains seen in the AFM images [Figs. 3(a)–3(d)] as well as published by others for *a*-axis $YBa_2Cu_3O_{7-x}$ grown on (100) $LaAlO_3$.[17,20,36,37,53,54] We know from the XRD ϕ-scans [Figs. 2(b) and S5] that there is an equal volume fraction of both 90° in-plane rotation twin variants, and although the volume sampled in our STEM investigation is small, this hypothesis is also consistent with our STEM observations. Once the substrate temperature is sufficiently high that the *a*-axis $YBa_2Cu_3O_{7-x}$ grains nucleate, both twin variants continue through the entire $YBa_2Cu_3O_{7-x}/PrBa_2Cu_3O_{7-x}/YBa_2Cu_3O_{7-x}$ trilayer.

Finally, in order to gain insights into the effect of *c*-axis grains in the trilayers, we perform additional cross-sectional STEM investigations on a less-ideal 32 nm/8 nm/32 nm sample. XRD shows the sample chosen to contain a higher volume fraction (16%) of *c*-axis oriented $YBa_2Cu_3O_{7-x}/PrBa_2Cu_3O_{7-x}$ (Fig. S8) and to have a higher rms roughness (> 1 nm) than the 32 nm/8 nm/32 nm trilayer characterized in Figs. 2–4. HAADF-STEM imaging (Fig. S9) of this less-ideal 32 nm/8 nm/32 nm trilayer confirms the presence of *c*-axis oriented grains in the structure and also demonstrates the rougher interfaces. Although the interfaces are rougher, STEM-EELS (Fig. S10) shows that they remain chemically abrupt. These results, when evaluated together, explain the rougher surfaces of the thicker samples. The formation of *c*-axis grains in the bottom $YBa_2Cu_3O_{7-x}$ layer not only disturbs the $PrBa_2Cu_3O_{7-x}$ layer (and interface) profiles, but also directly influences the top surface roughness by changing the local structural homogeneity in the first layers of the growth. The strong correlation between surface roughness and the volume fraction of *c*-axis grains in *a*-axis $YBa_2Cu_3O_{7-x}$ films has been previously noted.[42] To avoid *c*-axis oriented $YBa_2Cu_3O_{7-x}$, we initiate growth at a substrate temperature where only cubic $(Y,Ba)CuO_{3-x}$ can nucleate.

In conclusion, we revisited the growth of *a*-axis $YBa_2Cu_3O_{7-x}/PrBa_2Cu_3O_{7-x}/YBa_2Cu_3O_{7-x}$ trilayers and were able to improve their structural quality. By leveraging a temperature-ramping procedure that begins with a cubic $(Y,Ba)CuO_{3-x}$ buffer layer, we have grown high-quality *a*-axis trilayers as confirmed by *ex situ* XRD measurements. AFM investigations revealed an improved surface quality with an rms roughness that is less than ξ_a for the thinnest $YBa_2Cu_3O_{7-x}/PrBa_2Cu_3O_{7-x}/YBa_2Cu_3O_{7-x}$ trilayers. STEM analyses unveil the interrelation between *c*-axis

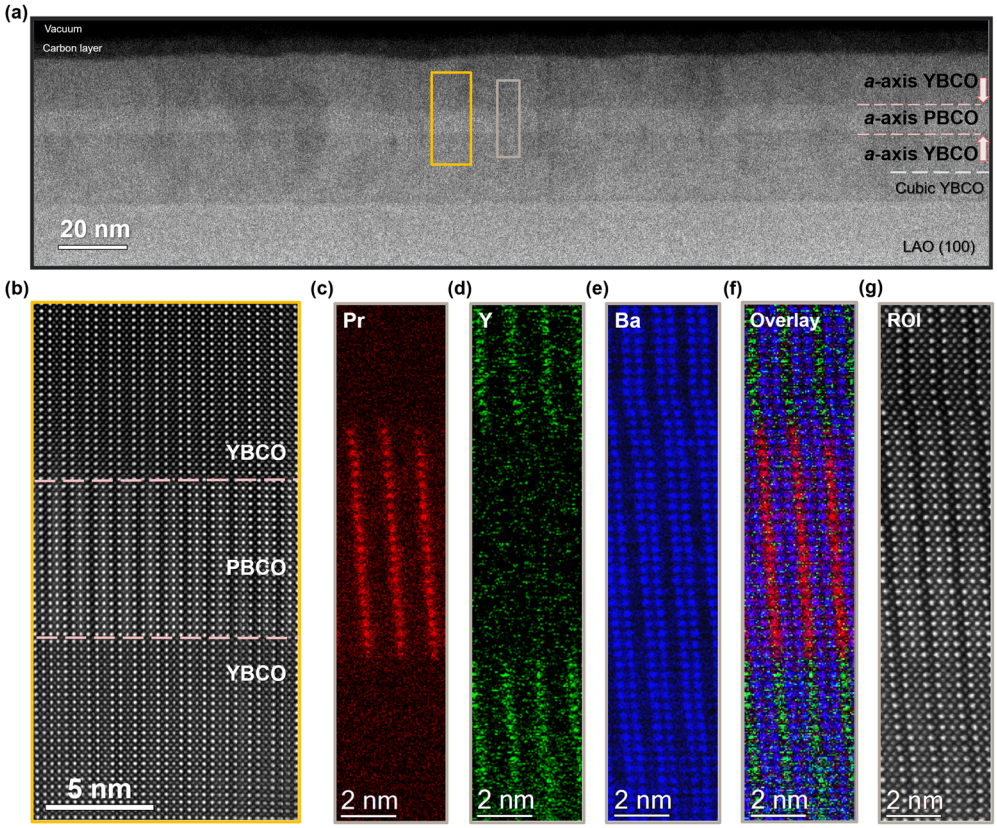

FIG. 5. (a) Low-magnification cross-sectional HAADF-STEM image of the 24 nm/8 nm/24 nm $YBa_2Cu_3O_{7-x}/PrBa_2Cu_3O_{7-x}/YBa_2Cu_3O_{7-x}$ trilayer revealing the microstructure and interface abruptness at the atomic scale. Individual $YBa_2Cu_3O_{7-x}$ and $PrBa_2Cu_3O_{7-x}$ layers are separated using dashed lines, and the pink arrows indicate the interfaces. (b) High-magnification scan of the area highlighted by the orange rectangle in (a) demonstrates that the interfaces are fully coherent. [(c)–(e)] Atomically resolved Pr–$M_{5,4}$ edge (red), Y–$L_{3,2}$ edge (green), and Ba–$M_{5,4}$ edge (blue) elemental maps evidencing the sharp chemical abruptness of the interfaces. (f) The RGB overlay and (g) the simultaneously acquired ADF-STEM image of the same region, outlined by the tan rectangle in (a).

oriented regions and surface roughness. Resistivity vs temperature measurements exhibit an onset of the superconducting transition at $T_{onset} \sim 85$ K and also the widening of the superconducting transition width with decreasing $YBa_2Cu_3O_{7-x}$ film thickness. Sharp and coherent interfaces with limited elemental intermixing are evidenced by atomic-resolution HAADF-STEM and STEM-EELS. Our findings suggest that with precise control of the growth conditions, the sharp interfaces and smooth surfaces required in *a*-axis-based $YBa_2Cu_3O_{7-x}$ heterostructures for high-performance Josephson junctions and other oxide electronics are within reach.

See the supplementary material for details on the flux calibration method conducted immediately prior to the growth of the $YBa_2Cu_3O_{7-x}/PrBa_2Cu_3O_{7-x}/YBa_2Cu_3O_{7-x}$ trilayers as well as additional characterization of the trilayers by RHEED, XRD, HAADF-STEM, and STEM-EELS.

AUTHORS' CONTRIBUTIONS

Y.E.S. and J.S. contributed equally to this work.

ACKNOWLEDGMENTS

This work was primarily supported by Ambature, Inc. B.H.G. and L.F.K. acknowledge support from the Department of Defense Air Force Office of Scientific Research (Grant No. FA 9550-16-1-0305). The authors thank Ronald Kelly, Michael Lebby, Davis Hartman, Mitch Robson, and Ivan Bozovic for fruitful discussions. This work made use of a Helios FIB supported by the NSF (Grant No. DMR-1539918) and the Cornell Center for Materials Research (CCMR) Shared Facilities, which are supported through the NSF MRSEC Program (Grant No. DMR-1719875). The authors acknowledge Malcolm Thomas, Donald Werder, John Grazul, and Mariena Silvestry Ramos for assistance in the Electron Microscopy CCMR facilities. The FEI Titan Themis 300 was acquired through Grant No. NSF-MRI-1429155, with additional support from Cornell University, the Weill Institute, and the Kavli Institute at Cornell. This work also made use of the CESI Shared Facilities partly sponsored by the NSF (Grant No. DMR-1338010) and the Kavli Institute at Cornell. Substrate preparation was performed, in part, at the Cornell NanoScale Facility, a member of the National Nanotechnology Coordinated Infrastructure (NNCI), which is supported by the NSF

(Grant No. NNCI-2025233). The authors thank Sean C. Palmer for his assistance with substrate preparation.

DATA AVAILABILITY

The data that support the findings of this study are available from the corresponding author upon reasonable request.

REFERENCES

[1]M. K. Wu, J. R. Ashburn, C. J. Torng, P. H. Hor, R. L. Meng, L. Gao, Z. J. Huang, Y. Q. Wang, and C. W. Chu, Phys. Rev. Lett. **58**, 908 (1987).
[2]R. J. Cava, B. Batlogg, R. B. van Dover, D. W. Murphy, S. Sunshine, T. Siegrist, J. P. Remeika, E. A. Rietman, S. Zahurak, and G. P. Espinosa, Phys. Rev. Lett. **58**, 1676 (1987).
[3]H.-C. Ri, R. Gross, F. Gollnik, A. Beck, R. P. Huebener, P. Wagner, and H. Adrian, Phys. Rev. B **50**, 3312 (1994).
[4]R. I. Rey, C. Carballeira, J. M. Doval, J. Mosqueira, M. V. Ramallo, A. Ramos-Álvarez, D. Sóñora, J. A. Veira, J. C. Verde, and F. Vidal, Supercond. Sci. Technol. **32**, 045009 (2019).
[5]B. Oh, K. Char, A. D. Kent, M. Naito, M. R. Beasley, T. H. Geballe, R. H. Hammond, A. Kapitulnik, and J. M. Graybeal, Phys. Rev. B **37**, 7861 (1988).
[6]J. B. Barner, C. T. Rogers, A. Inam, R. Ramesh, and S. Bersey, Appl. Phys. Lett. **59**, 742 (1991).
[7]R. Gross, L. Alff, A. Beck, O. M. Froehlich, D. Koelle, and A. Marx, IEEE Trans. Appl. Supercond. **7**, 2929 (1997).
[8]R. H. Koch, C. P. Umbach, G. J. Clark, P. Chaudhari, and R. B. Laibowitz, Appl. Phys. Lett. **51**, 200 (1987).
[9]J. E. Zimmerman, J. A. Beall, M. W. Cromar, and R. H. Ono, Appl. Phys. Lett. **51**, 617 (1987).
[10]J. Mannhart, P. Chaudhari, D. Dimos, C. C. Tsuei, and T. R. McGuire, Phys. Rev. Lett. **61**, 2476 (1988).
[11]D. Koelle, R. Kleiner, F. Ludwig, E. Dantsker, and J. Clarke, Rev. Mod. Phys. **71**, 631 (1999).
[12]H. Hilgenkamp and J. Mannhart, Rev. Mod. Phys. **74**, 485 (2002).
[13]S. A. Cybart, E. Y. Cho, T. J. Wong, B. H. Wehlin, M. K. Ma, C. Huynh, and R. C. Dynes, Nat. Nanotechnol. **10**, 598 (2015).
[14]J. Gao, Yu. Boguslavskij, B. B. G. Klopman, D. Terpstra, G. J. Gerritsma, and H. Rogalla, Appl. Phys. Lett. **59**, 2754 (1991).
[15]J. Gao, Yu. M. Boguslavskij, B. B. G. Klopman, D. Terpstra, R. Wijbrans, G. J. Gerritsma, and H. Rogalla, J. Appl. Phys. **72**, 575 (1992).
[16]H. Asano, M. Asahi, and O. Michikami, Jpn. J. Appl. Phys., Part 2 **28**, L981 (1989).
[17]C. B. Eom, A. F. Marshall, S. S. Laderman, R. D. Jacowitz, and T. H. Geballe, Science **249**, 1549 (1990).
[18]I. Takeuchi, P. A. Warburton, Z. Trajanovic, C. J. Lobb, Z. W. Dong, T. Venkatesan, M. A. Bari, W. E. Booij, E. J. Tarte, and M. G. Blamire, Appl. Phys. Lett. **69**, 112 (1996).
[19]F. Miletto Granozio and U. S. di Uccio, J. Cryst. Growth **174**, 409 (1997).
[20]A. Inam, C. T. Rogers, R. Ramesh, K. Remschnig, L. Farrow, D. Hart, T. Venkatesan, and B. Wilkens, Appl. Phys. Lett. **57**, 2484 (1990).
[21]Z. Trajanovic, I. Takeuchi, P. A. Warburton, C. J. Lobb, and T. Venkatesan, Appl. Phys. Lett. **66**, 1536 (1995).
[22]A. Inam, R. Ramesh, and C. T. Rogers, U.S. patent 5,324,714 (28 June 1994).
[23]A. Inam, R. Ramesh, and C. T. Rogers, U.S. patent 5,358,927 (25 October 1994).
[24]I. Bozovic, J. N. Eckstein, N. Bozovic, and J. O'Donnell, MRS Online Proc. Libr. Arch. **502**, 221 (1997).
[25]I. Bozovic, J. N. Eckstein, and N. Bozovic, *In Situ Process Diagnostics and Intelligent Materials Processing* (Wiley Science, 2000), pp. 29–56.
[26]B. A. Davidson, R. Ramazashvili, S. Kos, and J. N. Eckstein, Phys. Rev. Lett. **93**, 107004 (2004).
[27]J. N. Eckstein, M. Zheng, X. Zhai, B. Davidson, M. Warusawithana, and S. Oh, in *Molecular Beam Epitaxy From Research to Mass Production* (Elsevier, Inc., 2013), pp. 509–528.
[28]R. Baghdadi, R. Arpaia, E. Stepantsov, M. Arzeo, D. Golubev, D. Montemurro, E. Andersson, T. Bauch, and F. Lombardi, Phys. Rev. B **95**, 184505 (2017).
[29]G. W. Berkstresser, A. J. Valentino, and C. D. Brandle, J. Cryst. Growth **128**, 684 (1993).
[30]P. D. C. King, H. I. Wei, Y. F. Nie, M. Uchida, C. Adamo, S. Zhu, X. He, I. Božović, D. G. Schlom, and K. M. Shen, Nat. Nanotechnol. **9**, 443 (2014).
[31]M. Park, M. J. Kramer, K. W. Dennis, and R. W. McCallum, Physica C **259**, 43 (1996).
[32]J. A. Edwards, N. G. Chew, S. W. Goodyear, J. S. Satchell, S. E. Blenkinsop, and R. G. Humphreys, J. Less-Common Met. **164-165**, 414 (1990).
[33]J. A. Agostinelli, S. Chen, and G. Braunstein, Phys. Rev. B **43**, 11396 (1991).
[34]M. Bosman, M. Watanabe, D. T. L. Alexander, and V. J. Keast, Ultramicroscopy **106**, 1024 (2006).
[35]C. Giacovazzo, H. L. Monaco, G. Artioli, D. Viterbo, G. Ferraris, G. Gilli, G. Zanotti, and M. Catti, *Fundamentals of Crystallography*, 2nd ed. (Oxford University Press, Oxford, NY, 2002), pp. 335–338.
[36]R. Ramesh, A. Inam, D. M. Hwang, T. S. Ravi, T. Sands, X. X. Xi, X. D. Wu, Q. Li, T. Venkatesan, and R. Kilaas, J. Mater. Res. **6**, 2264 (1991).
[37]A. F. Marshall and C. B. Eom, Physica C **207**, 239 (1993).
[38]H. M. Appelboom, V. C. Matijasevic, F. Mathu, G. Rietveld, B. Anczykowski, W. J. A. M. Peterse, F. Tuinstra, J. E. Mooij, W. G. Sloof, H. A. Rijken, S. S. Klein, and L. J. van Ijzendoorn, Physica C **214**, 323 (1993).
[39]J. A. Agostinelli, S. Chen, and G. Braunstein, Physica C **180**, 26 (1991).
[40]S. W. Chan, D. M. Hwang, and L. Nazar, J. Appl. Phys. **65**, 4719 (1989).
[41]P. Berberich, B. Utz, W. Prusseit, and H. Kinder, Physica C **219**, 497 (1994).
[42]T. Umezawa, D. J. Lew, S. K. Streiffer, and M. R. Beasley, Appl. Phys. Lett. **63**, 3221 (1993).
[43]J. Wu, O. Pelleg, G. Logvenov, A. T. Bollinger, Y.-J. Sun, G. S. Boebinger, M. Vanević, Z. Radović, and I. Božović, Nat. Mater. **12**, 877 (2013).
[44]M. Tinkham, *Introduction to Superconductivity*, 2nd ed. (McGraw Hill, New York, 1996), pp. 148–195.
[45]M. V. Ramallo and F. Vidal, Physica C **282-287**, 1541 (1997).
[46]D. Putzky, P. Radhakrishnan, Y. Wang, P. Wochner, G. Christiani, M. Minola, P. A. van Aken, G. Logvenov, E. Benckiser, and B. Keimer, Appl. Phys. Lett. **117**, 072601 (2020).
[47]S. J. Pennycook, Ultramicroscopy **30**, 58 (1989).
[48]Y. E. Suyolcu, Y. Wang, F. Baiutti, A. Al-Temimy, G. Gregori, G. Cristiani, W. Sigle, J. Maier, P. A. van Aken, and G. Logvenov, Sci. Rep. **7**, 453 (2017).
[49]Y. E. Suyolcu, G. Christiani, P. A. van Aken, and G. Logvenov, J. Supercond. Novel Magn. **33**, 107 (2020).
[50]H. W. Zandbergen, R. Gronsky, K. Wang, and G. Thomas, Nature **331**, 596 (1988).
[51]R. Ramesh, D. M. Hwang, J. B. Barner, L. Nazar, T. S. Ravi, A. Inam, B. Dutta, X. D. Wu, and T. Venkatesan, J. Mater. Res. **5**, 704 (1990).
[52]H. Zhang, N. Gauquelin, G. A. Botton, and J. Y. T. Wei, Appl. Phys. Lett. **103**, 052606 (2013).
[53]S. K. Streiffer, B. M. Lairson, E. M. Zielinski, and J. C. Bravman, Phys. Rev. B **47**, 11431 (1993).
[54]S. K. Streiffer, B. M. Lairson, E. M. Zielinski, and J. C. Bravman, MRS Online Proc. Libr. Arch. **275**, 771 (1992).